

THE COMPRESSION OF THE M-0.02-0.07 MOLECULAR CLOUD BY THE SAGITTARIUS A EAST SHELL SOURCE

E. SERABYN¹

California Institute of Technology, 320-47, Pasadena, CA 91125

AND

J. H. LACY¹ AND J. M. ACHTERMANN¹

Department of Astronomy, University of Texas, Austin, TX 78712

Received 1991 November 15; accepted 1992 February 14

ABSTRACT

The “50 km s⁻¹” molecular cloud (M-0.02-0.07) near the Galactic center has been mapped in the CS $J = 7-6$ and $5-4$ rotational transitions. In addition, mid-infrared fine-structure lines of [Ne II], [Ar III], and [S IV] have been observed toward the compact H II regions located near the cloud’s core. We find the following: (1) A dense molecular layer, with $n \sim 1-2 \times 10^6$ cm⁻³, curves around the entire eastern half of the Sgr A East shell source, implying that Sgr A East is impacting upon and compressing this molecular cloud. No corresponding molecular layer is seen on the opposite side of Sgr A East. (2) Just inside of this curved ridge, highly red- and blueshifted gas is seen, which has likely been accelerated by the blast wave. (3) Just to the east of this compressed ridge lies the true molecular cloud core, as well as the string of compact H II regions Sgr A East-A through D. Since the compression wave has not yet reached either the cloud core or the compact H II regions, they must be due to an episode of collapse and star formation which occurred prior to the impact of Sgr A East. (4) The sources exciting the compact H II regions have spectra and luminosities corresponding approximately to O8–O9 stars. These results suggest a two-component model for the dense gas in M-0.02-0.07: a normal, dense, star-forming cloud core, and a compression wave which has advanced into the cloud from the direction of Sgr A East.

Subject headings: Galaxy: center — H II regions — ISM: individual (M-0.02-0.07) — ISM: molecules — supernovae remnants

1. INTRODUCTION

The “50 km s⁻¹ cloud,” or M-0.02-0.07 (Güsten, Walmsley, & Pauls 1981; Brown & Liszt 1984; Liszt, Burton, & van der Hulst 1985; Güsten 1989), is a massive molecular cloud which lies, in projection, within 2'–3' of the center of our Galaxy. Since this cloud harbors a string of compact H II regions near its center (Ekers et al. 1983; Goss et al. 1985; Yusef-Zadeh & Morris 1987), M-0.02-0.07 may be one of the nearest sites of star formation to the center of our Galaxy. As such, it can provide a unique window on the process of star formation in the vicinity of a galactic nucleus.

Star formation in the vicinity of M-0.02-0.07 is also suggested by the proximity of Sgr A East, a nonthermal radio shell source (Ekers et al. 1983; Liszt et al. 1985; Ho et al. 1985; Sandqvist 1989; Goss et al. 1989; Pedlar et al. 1989), which shows some of the characteristics of a supernova remnant (SNR), but which on the other hand may be more energetic than a typical SNR (Mezger et al. 1989), and so may require multiple stellar winds and explosions (i.e., a “superbubble”), or some Seyfert-like activity. Regardless of its nature, the detection of a ridge of dust and dense molecular gas to the east of the radio shell has provided good evidence for an interaction between the expanding shell and the molecular material (Mezger et al. 1989; Zylka, Mezger, & Wink 1990; Zylka 1990; Genzel et al. 1990; Ho et al. 1991). However, the extant molecular observations have not yet yielded a complete picture of

this interaction, primarily because the field involved is large, and the spectra of low-excitation transitions are complicated by additional features.

To improve our understanding of the relationships between (1) the core of the 50 km s⁻¹ cloud, (2) the compact H II regions A–D located near this cloud core, (3) the Sgr A East radio continuum shell, and (4) the molecular and dust ridge seen just outside of the Sgr A East shell, new molecular and ionic line observations were undertaken. Since compressed regions and cloud cores necessarily imply high densities, such regions are best studied with a density-sensitive molecule such as CS, which has already proven very useful in distinguishing gas components at the Galactic center from foreground material (e.g., Serabyn & Güsten 1987; Bally et al. 1988; Stark et al. 1989; Tsuboi et al. 1989, 1991). M-0.02-0.07 was therefore mapped in the CS $J = 5-4$ and $7-6$ rotational transitions at the Caltech Submillimeter Observatory (CSO).

In addition, infrared fine-structure line observations were used as probes of the ionized gas in the compact H II regions. Based on their radio emission measures and spectral indices, as well as the presence of emission lines of H and Ne⁺ (Ekers et al. 1983; Serabyn 1984; Goss et al. 1985; Pedlar et al. 1989), it has generally been concluded that these H II regions are photoionized (see, however, Yusef-Zadeh & Morris 1987). In order to better characterize the spectra of the excitation sources, fine-structure lines of Ne⁺, Ar⁺⁺, and S⁺³ were observed at the IRTF.

2. CS DISTRIBUTION AND KINEMATICS

Maps in the CS $J = 7-6$ and $5-4$ lines, as well as a single spectrum of the C³⁴S $5-4$ transition, were obtained using the

¹ Visiting Astronomer at the Infrared Telescope Facility, which is operated by the University of Hawaii under contract with the National Aeronautics and Space Administration.

TABLE 1
CS OBSERVING PARAMETERS

Transition	Frequency (GHz)	Observation Date	Beam	Number of Positions	Grid Spacing	Efficiency η_{mb}	T_{rec} (K)	Resolution (km s ⁻¹)
CS (7-6)	342.882 949	1991 Aug	20"	66	30"	0.6	300	0.48
CS (5-4)	244.935 606	1990 Aug	29	151	30	0.7	400	0.60
C ³⁴ S (5-4)	241.016 176	1990 Nov	29	1	...	0.7	400	0.61

facility SIS receivers and acousto-optical spectrometers of the CSO. The observing parameters are summarized in Table 1, and the positions measured are indicated in Figure 5. Positional offsets are referred to Sgr A*, the radio point source at the center of Sgr A West (Lo 1989). The pointing, as verified on IRAS 16293-2422 and Saturn, was accurate to better than 5".

Since the maps in both the CS 5-4 and 7-6 transitions were very similar in appearance, but the 5-4 map showed a substantially higher signal-to-noise ratio, we present these results first. Figure 1 shows a subset of the acquired 5-4 spectra encompassing the center of the area mapped. At most positions on the grid, the observed lines consist primarily of a single strong velocity component. The strongest lines are centered at ≈ 45 km s⁻¹ LSR, but across the field the line-center velocity varies

over the range 25-65 km s⁻¹. The linewidth of this emission is ≈ 20 -30 km s⁻¹ FWHM, which clearly places this cloud in the central few hundred parsec region of our Galaxy (Güsten 1989; Stark et al. 1989).

In addition, a few localized areas in Figure 1 show a second, usually much weaker velocity component. First, in several positions toward the western edge of the spectral grid, the circumnuclear disk surrounding Sgr A West (Genzel & Townes 1987) is weakly seen at high positive and negative velocities. Second, in a few positions toward the northern extremity of the map, a distinct velocity component near 0 km s⁻¹ is present. This emission may be related to a gas feature which extends northward from the vicinity of Sgr A toward the arched filaments (Serabyn & Güsten 1987; Genzel et al. 1990). Finally, in a few spectra near the center of the map, weak blue- and redshifted emission components can be seen to either side of the main 45 km s⁻¹ emission (at $\Delta\alpha = 95''$, $\Delta\delta = -30''$ to $+60''$). The latter emission is discussed in § 5. In general, compared to the strong emission near 45 km s⁻¹, all of these secondary components are either very weak or localized, and thus there is no ambiguity in identifying the correct velocity feature with the 50 km s⁻¹ cloud.

The observed 5-4 emission, integrated over two velocity intervals broad enough to encompass nearly all of the emission seen, is shown superposed on the radiograph of Sgr A presented by Pedlar et al. (1989) in Figure 2 (Plate 2). In this radiograph, which is color coded by spectral index, the thermal Sgr A West H II region, and the Sgr A East compact H II regions A-D appear yellow to red, while the nonthermal Sgr A East shell appears in blue. The solid contours (20-80 km s⁻¹) show mainly the CS emission from M-0.02-0.07, but near Sgr A West the northern half of the circumnuclear disk is also seen, as mentioned above. The dashed contours (-100 to -40 km s⁻¹) show the opposite half of this disk. Although the northern half of the disk seems to be connected to M-0.02-0.07, this might also be the result of limited spatial resolution.

In Figure 2, the emission from M-0.02-0.07 is seen to consist primarily of a molecular ridge which curves around the eastern side of the Sgr A East radio continuum shell, as well as an emission maximum located just eastward of this ridge, at about $(\Delta\alpha, \Delta\delta) \approx (180'', 90'')$. Since the CS ridge curves around nearly half of the Sgr A East shell, this juxtaposition indicates clearly that Sgr A East is interacting with the 50 km s⁻¹ cloud. The best explanation, as discussed previously by many authors, is that Sgr A East is impacting upon, and compressing, the M-0.02-0.07 cloud.

The relationship between this CS ridge and the peak just to its east is not clear from Figure 2 alone, but is clarified with the aid of kinematic information. To this end, Figure 3 presents the CS 5-4 emission in 10 km s⁻¹ wide channels, and Figure 4 presents a series of parallel declination-velocity (δ - v) plots across the map. In the channel maps, the peak and ridge are distinguishable in that the peak is present in nearly the same location in the five channel maps in which it is seen (25-65 km

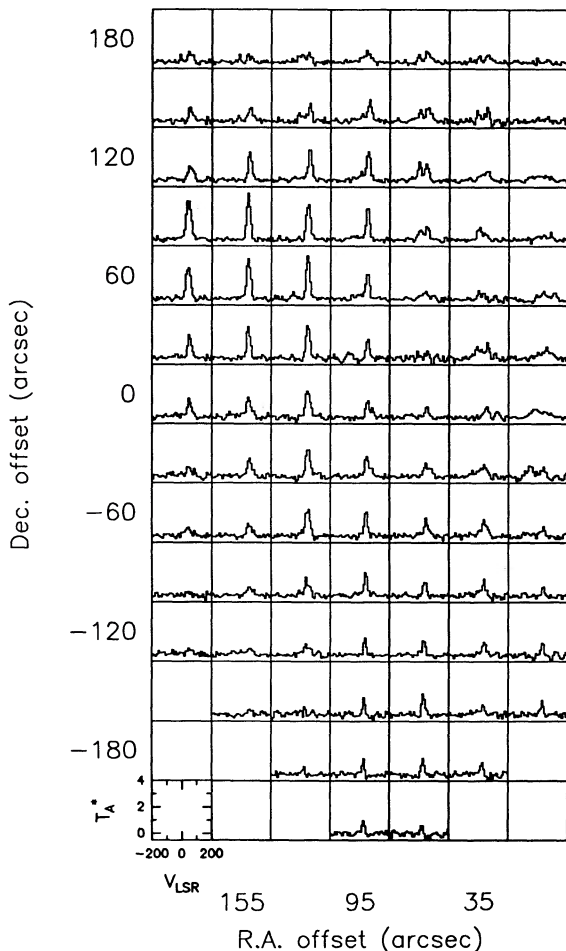


FIG. 1.—Grid of CS $J = 5-4$ spectra observed toward the eastern half of Sgr A East. The grid spacing is 30", and the angular offsets are relative to Sgr A*. Velocity and temperature scales for all spectra are given in the lower left corner.

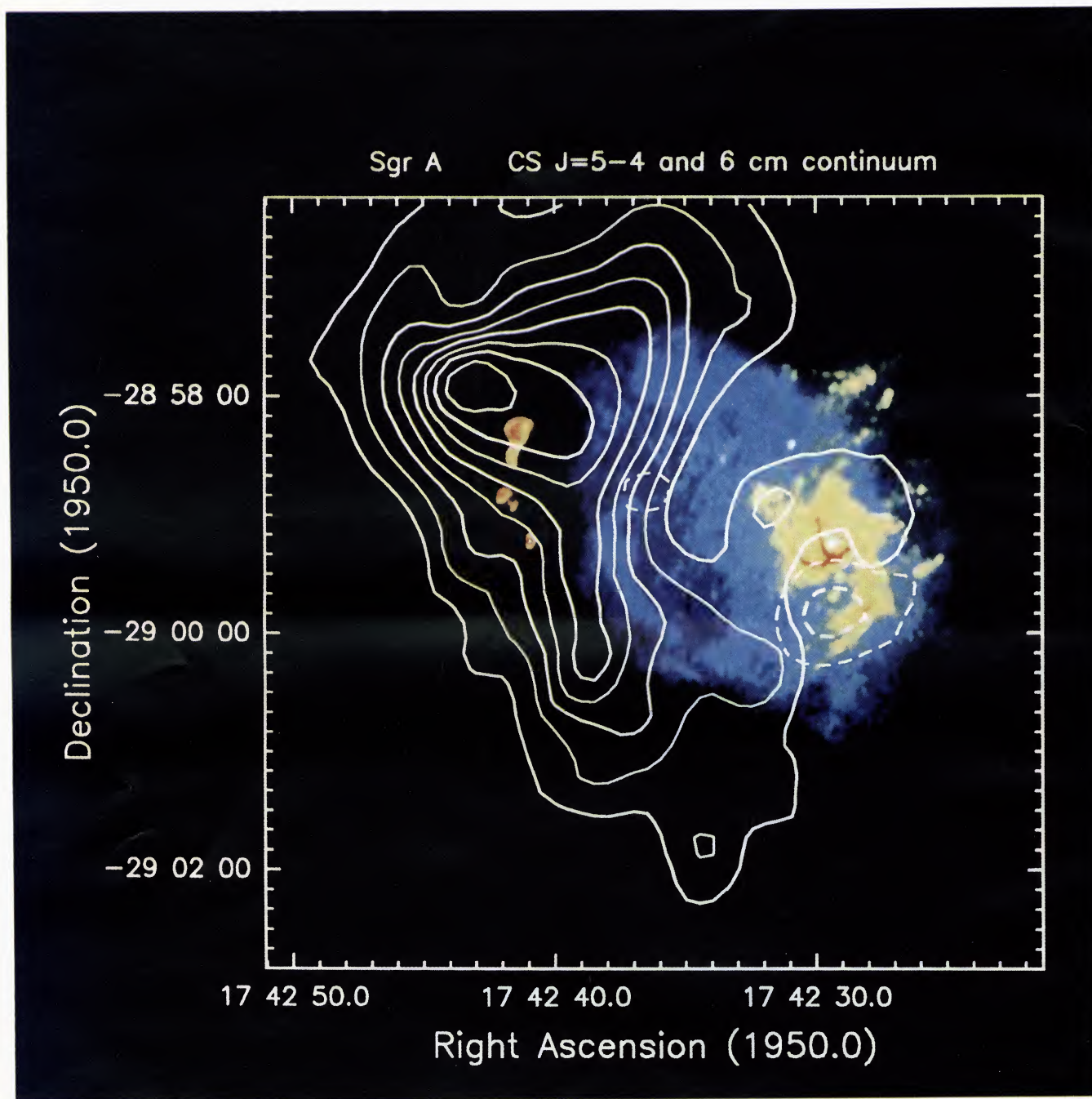


FIG. 2.—Overlay of the CS $J = 5-4$ emission contours from M-0.02-0.07 and the circumnuclear disk on the radiograph of Sgr A of Pedlar et al. (1989). Except for small areas in the two lower corners (see Fig. 5), the entire field has been mapped in CS 5-4. The solid (dashed) contours are for $20 < v < 80 \text{ km s}^{-1}$ ($-100 < v < -40 \text{ km s}^{-1}$), with levels (in units of T^*_mb) of 24 to 108 K km s^{-1} by 12 K km s^{-1} . One σ equals 4 K km s^{-1} . The color radiograph has intensities proportional to the 6 cm flux, and colors dependent on the radio spectral index (Pedlar et al.). Thus, the nonthermal Sgr A East shell source appears in blue, the thermal Sgr A West region (toward the right) appears yellow/red, and the four Sgr A East compact H II regions (on the left) are red/orange (from north to south, A, B, C, and D, with A and B partially blended; see Goss et al. 1985 for details).

SERABYN, LACY & ACHTERMANN (see 395, 167)

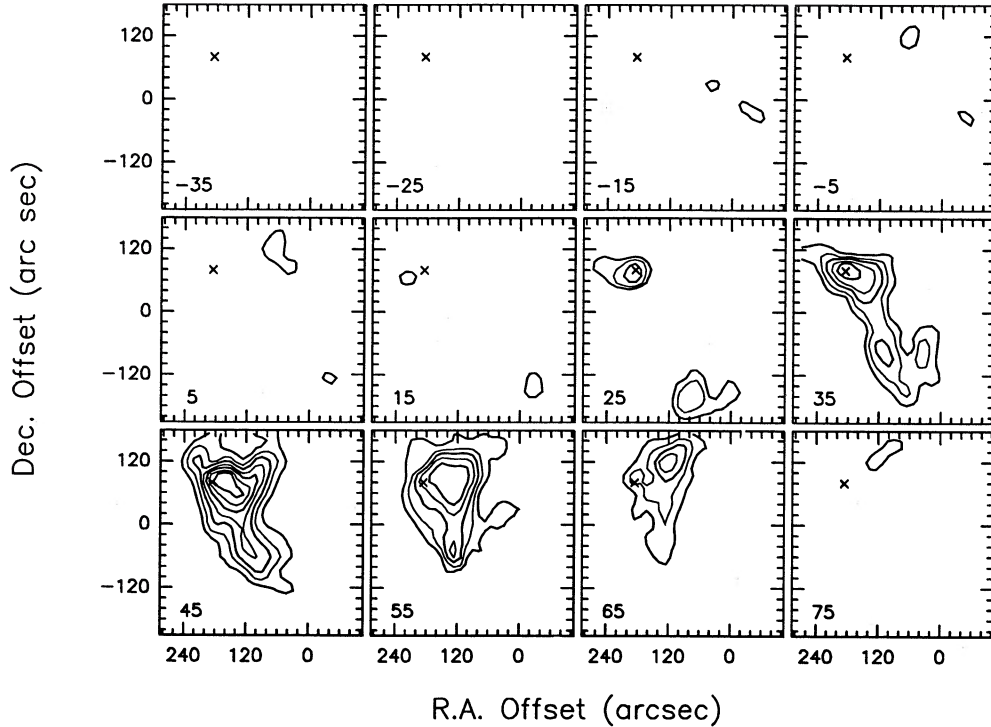


FIG. 3.—Contour maps of the CS $J = 5-4$ emission integrated over 10 km s^{-1} wide channels, centered on -35 to 75 km s^{-1} . The contour levels, in units of T_{A}^* , are 8, 12, 16 ... K km s^{-1} , and $\sigma = 1.4 \text{ K km s}^{-1}$. The cross in each panel at $(185'', 80'')$ is a reference mark near the cloud peak.

s^{-1}), while the ridgelike component advances steadily across the field from south to north in the same five channels. The $\delta-v$ cuts show the same $\approx 40 \text{ km s}^{-1}$ velocity shift along the main CS ridge (α offsets of $65''-125''$), but not further east. Thus, while a velocity gradient of $5-6 \text{ km s}^{-1} \text{ arcmin}^{-1}$ is present along the main CS ridge, only a rather constant velocity is seen near the cloud peak. Of course, the latter may simply be due to the peak's localized nature. Note that the full velocity shift seen across the cloud is only somewhat larger than the 30 km s^{-1} line width at the cloud peak.

Returning to Figure 2, several additional aspects of the M-0.02-0.07 cloud are also evident. First, the compact H II regions A-D are located just outside of the dense CS ridge (opposite to the side of Sgr A East), and just south of the CS emission maximum. Second, the eastern edge of M-0.02-0.07 is

seen to be approximately aligned with the galactic plane, possibly reflecting the cloud's initial (predisturbance) orientation. Third, in the lower Galactic longitude direction of the neighboring " 20 km s^{-1} cloud," or M-0.13-0.08 (Güsten 1989; Sandqvist 1989; Okumura et al. 1989, 1991; Zylka 1990), the CS emission becomes very weak, but does not fade away completely. Finally, since the compressed 50 km s^{-1} material is seen only in a narrow band to the east of Sgr A East, the areal covering factor of the radio shell by molecular material is very low, $\lesssim 0.2$. Thus, either the shell has broken out of the molecular cloud to a large extent, or it originated outside of the cloud. In this regard, note that the halo of nonthermal emission surrounding parts of the Sgr A East shell (Yusef-Zadeh & Morris 1987; Pedlar et al. 1989) lies, in large part, to the west of Sgr A East, just the direction where the molecular CS emission is

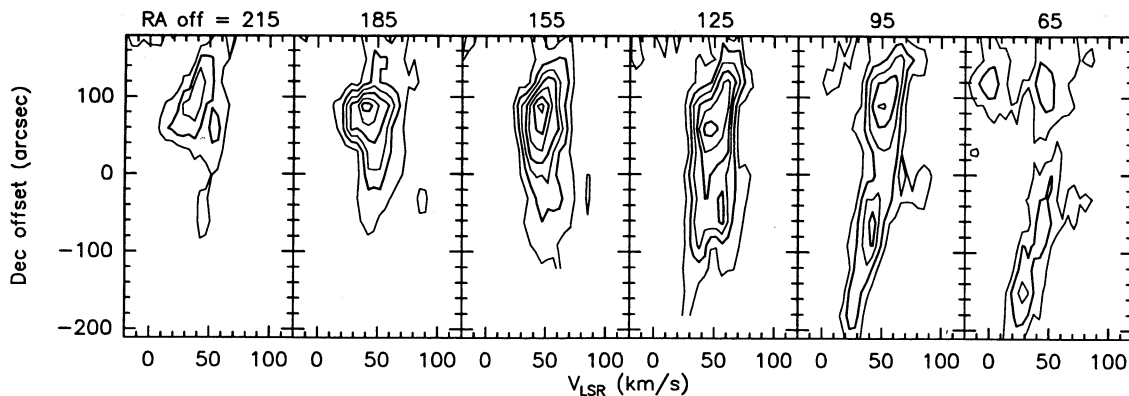


FIG. 4.—Declination-velocity plots of the CS $J = 5-4$ emission along cuts spaced by $30''$ in right ascension. Contour levels are 0.5, 1.0, 1.5 ... K . The three rightmost panels cross Sgr A East, but the three leftmost panels do not.

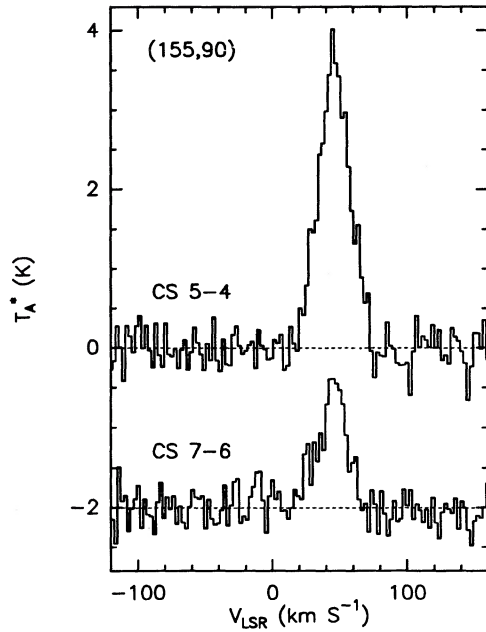


FIG. 5.—CS $J = 7-6$ and $J = 5-4$ spectra toward $(\Delta\alpha, \Delta\delta) = (155'', 90'')$, close to the cloud peak. Both spectra are binned to the same resolution of 2.4 km s^{-1} .

weak (compare our Fig. 2 to Fig. 5 of Pedlar et al.). Thus, the halo may be related to regions of more rapid breakout from the confining molecular gas.

Comparing to previous observations, the observed combination of a basically N-S ridge along the eastern side of Sgr A East, with another peak to its east, reproduces very well the main features of the dust distribution seen to the east of the Sgr A East shell (Mezger et al. 1989). However, no corresponding CS counterpart is seen on the opposite, western, side of Sgr A East. Since dust continuum emission does not contain kinematic information, the proposed nearly-complete "ring" of dust around Sgr A East (Mezger et al.) may thus be due to a superposition of a number of different molecular features, including M-0.13-0.08 in the south (e.g., Okumura et al. 1991),

the Sgr A West circumnuclear disk in the southwest, and the -20 km s^{-1} cloud (Serabyn & Güsten 1987; Genzel et al. 1990) in the north. Alternatively, the swept-up gas could be more tenuous, and perhaps even atomic, on the western side of the shell, and so not detectable in these highly excited CS lines.

The dense ridge east of Sgr A East has also been seen in other molecular lines (Zylka et al. 1990; Zylka 1990; Genzel et al. 1990; Ho et al. 1991), and the more spatially extended ^{13}CO data of Zylka et al. also show the eastern peak situated beyond this ridge. A molecular feature with orientation and kinematics very similar to those of our CS ridge was seen in ^{13}CO by Zylka et al. (their "streamer"). Because of the multiple velocity features seen in ^{13}CO , a unique identification of the "streamer" was difficult, but Zylka et al. suggested that, because of its larger than average velocity gradient, the "streamer" is separate from the 50 km s^{-1} cloud/Sgr A East complex, being instead an extension of the more southerly 20 km s^{-1} cloud across the field of Sgr A East. In contrast, since in our CS data the corresponding CS ridge (1) wraps directly around Sgr A East, (2) is the only feature present in the vicinity of the 50 km s^{-1} cloud, and (3) fades away toward the southern cloud, we conclude instead that the ridge/streamer is associated both with the 50 km s^{-1} cloud and Sgr A East, but not with the 20 km s^{-1} cloud. Since there is good evidence that Sgr A East is behind the Sgr A West H II region at the center of our Galaxy (e.g., Pedlar et al. 1989), the 50 km s^{-1} cloud must then also be located behind the center.

3. CS 7-6 EMISSION AND THE MOLECULAR DENSITY AND MASS

Figure 5 shows the CS 5-4 and 7-6 spectra observed toward $(\Delta\alpha, \Delta\delta) = (155'', 90'')$, just between the main cloud peak and the ridge seen in Figure 2. In Figure 6 the 7-6 and 5-4 intensities integrated over most of the line, $20-60 \text{ km s}^{-1}$, are compared side by side. Also shown are both observing grids. This velocity interval is somewhat smaller than that of Figure 2, in order to exclude, as much as possible, the emission from the circumnuclear disk. The spatial distributions of both lines are very similar, each showing the dense ridge curving down the center of the regions mapped, and also the peak just east of the

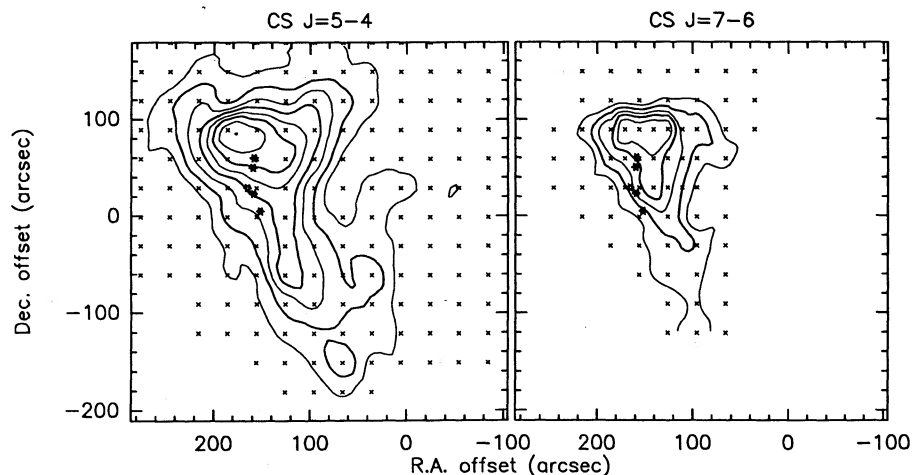


FIG. 6.—Contour maps of the CS $J = 5-4$ and $J = 7-6$ lines integrated over the range $20-60 \text{ km s}^{-1}$. The contour levels are 20, 30 to 102 by 12 K km s^{-1} for CS $J = 5-4$, and 12-36 by 6 K km s^{-1} for CS $J = 7-6$ (in units of T_A^*). The small crosses show the observing grid, and the five small stars show the Sgr A East compact H II regions (A, B, C1, C2, and D, from north to south). The field within the borders corresponds exactly to the boxed field presented in Fig. 5.

ridge at $(\Delta\alpha, \Delta\delta) \approx (180'', 90'')$. The 7–6 map differs from the 5–4 map mainly by a scaling factor of roughly 0.4 in T_A^* .

As a check on the CS line opacities, the $C^{34}S$ 5–4 line was also observed toward $(\Delta\alpha, \Delta\delta) = (155, 90)$. It was not detected, to a limit of ~ 0.2 K, implying that the CS lines are optically thin ($\tau_{5-4} < 0.6$). This allows straightforward density and mass estimates. For such extended sources the observed 7–6/5–4 line ratio can be corrected to the intrinsic source ratio by multiplying by the main-beam efficiency ratio (Table 1), yielding a corrected line ratio of 0.47. Assuming a kinetic temperature of 70 K for the molecular material (Güsten 1989), the optically thin case implies a density of $\approx 1.5 \pm 0.5 \times 10^6 \text{ cm}^{-3}$. For a CS abundance of 3×10^{-9} (Blake et al. 1987), this yields an H_2 column density through the cloud peak of $\sim 2 \times 10^{23} \text{ cm}^{-2}$, corresponding to $A_V \sim 200$. The ridge itself has values lower than these by up to a factor of ~ 2 . The total cloud mass in the dense component is then $1.5 \times 10^5 M_\odot$. These parameters are very similar to those estimated for the streamer/ridge by Zylka et al. (1990) and Genzel et al. (1990).

With the column density given, and a typical scale size of about $1'$, or 2.5 pc, the volume-averaged density is about $3 \times 10^4 \text{ cm}^{-3}$, a factor of about 50 lower than the measured local density. Near the cloud peak, this is likely due to the usual causes of small-scale clumping and consequent beam dilution, but for the compressed ridge adjacent to Sgr A East, a sheetlike geometry surrounding the expanding shell provides a very natural explanation.

4. INFRARED FINE-STRUCTURE LINES AND THE COMPACT H II REGIONS

Infrared fine-structure lines of $[Ne \text{ II}]$, $[S \text{ IV}]$ and $[Ar \text{ III}]$ at 12.8, 10.5, and 9.0 μm were observed toward the Sgr A East compact H II regions (A–D in north to south order, using the nomenclature of Goss et al. 1985) in July 1989 with Irshell, a mid-infrared cryogenic echelle spectrograph (Lacy et al. 1989b) on the NASA IRTF. Irshell uses a detector array to measure a 64 point spectrum of each of 10 positions spaced by $1''$ on the sky (in an East-West orientation for these observations). The spectral dispersions per pixel for the three lines were 0.043, 0.048, and 0.051 cm^{-1} , respectively. The spectral and spatial resolutions were both 2 pixels FWHM, and the pointing uncertainty $\sim 1''$. The sky background was subtracted with the IRTF chopping secondary, and calibration was on a dome-temperature blackbody.

$[Ne \text{ II}]$ and $[Ar \text{ III}]$ were observed toward all four compact H II regions, but $[S \text{ IV}]$ was observed only toward the strongest source, A, where it was not detected. Spectra obtained by summing along the observing slits are shown in Figure 7. Line fluxes, determined from peak brightnesses and observed source sizes, assuming Gaussian source profiles, are given in Table 2. In addition to the uncertainty in estimating the source shapes, pointing errors could result in underestimates of the line fluxes.

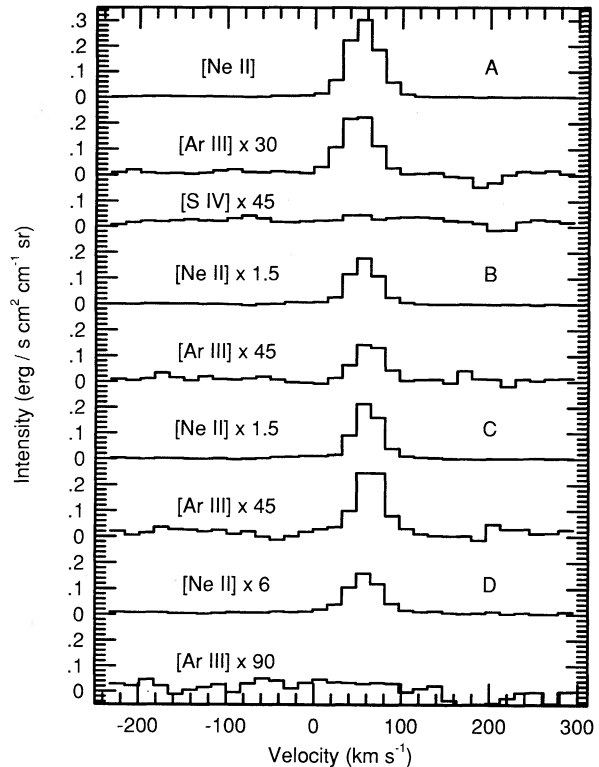


FIG. 7.— $[Ne \text{ II}]$, $[Ar \text{ III}]$, and $[S \text{ IV}]$ spectra toward the Sgr A East compact H II regions, averaged along the $1'' \times 10''$ east-west slit.

Also listed in Table 2 are the observed velocities. The velocities range between 43 and 49 km s^{-1} , and are consistent with the H 76 α velocities of Goss et al. (1985). As pointed out by Goss et al., the agreement between these velocities and the velocity of the molecular emission in this direction ($\sim 45 \text{ km s}^{-1}$) argues that the compact H II regions are associated with M-0.02-0.07. An East-West velocity gradient of about $1.5 \text{ km s}^{-1} \text{ arcsec}^{-1}$ (red to the east) was seen toward sources A and B, and a velocity-right ascension diagram for source A is shown in Figure 8. No significant gradients were seen toward sources C1, C2 and D.

The 5 GHz VLA maps of Yusef-Zadeh & Morris (1987) show sources A and B to be asymmetric shell sources, which may be an indication that the H II regions have broken out of the molecular clouds on the western side. Our observed velocity gradients are consistent with this picture if the sources are near the front surface of M-0.02-0.07. From their morphologies and lack of velocity shifts, sources C1 and C2 appear to be parts of a single slightly irregular shell, and source D appears to be at an earlier stage of evolution, still contained in the molecular cloud. The CS peak in Figure 2 could be another element in this chain, at a still earlier stage of evolution.

TABLE 2
IR FINE-STRUCTURE LINE OBSERVATIONS OF THE COMPACT H II REGIONS

Source	Size	Flux $[Ne \text{ II}]$ ($\text{ergs s}^{-1} \text{ cm}^{-2}$)	Flux $[Ar \text{ III}]$ ($\text{ergs s}^{-1} \text{ cm}^{-2}$)	Flux $[S \text{ IV}]$ ($\text{ergs s}^{-1} \text{ cm}^{-2}$)	$V_{LSR}([Ne \text{ II}])$ (km s^{-1})
A.....	10"	9.0 (–11)	1.7 (–12)	<2 (–13)	43
B.....	8	2.6 (–11)	5.5 (–13)	...	46
C.....	10	3.0 (–11)	1.0 (–12)	...	46
D.....	3.5	2.3 (–12)	<3.0 (–14)	...	45

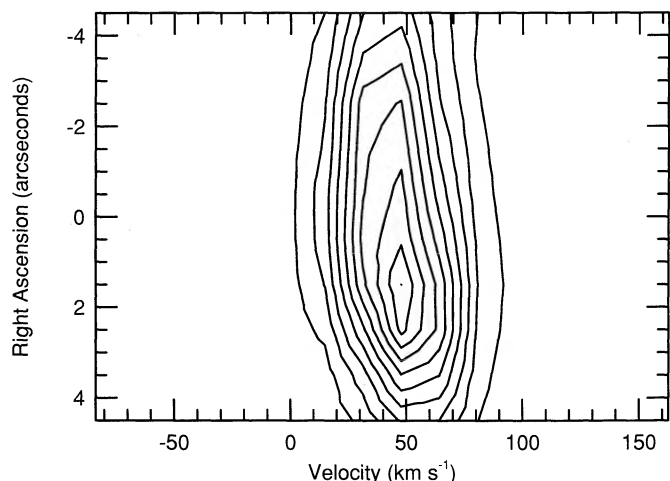


FIG. 8.—[Ne II] R.A.-velocity diagram across the compact H II region A. The contour levels are in steps of 10% of the peak. The resolutions are $2''$ spatial and 33 km s^{-1} spectral.

Ionic abundance ratios, Ne^+/H^+ , $\text{Ar}^{++}/\text{H}^+$, and S^{+3}/H^+ , for each of the compact H II regions, calculated using the collision strengths in Osterbrock (1989) and the 15 GHz free-free fluxes of Goss et al. (1985), but neglecting extinction, are given in Table 3, columns (3)–(5). Fractional ionic abundances, Ne^+/Ne , Ar^{++}/Ar , and S^{+3}/S , assuming total Ne, Ar, and S abundances twice (Lester et al. 1981; Lacy et al. 1989a) those found in Orion (Rubin 1985), are given in columns (6)–(8). The resultant Ne^+/Ne ratios are ~ 0.35 toward sources A–C and ~ 0.05 toward D. Since neon is predominantly singly ionized in H II regions for a wide range in stellar temperatures (Rubin), we attribute the apparent reduction in Ne^+/Ne to an extinction of ~ 1 mag toward sources A–C (Table 3, col. [9]), about equal to that seen toward Sgr A West (Becklin et al. 1978; Rieke & Lebofsky 1985). An additional ~ 2 mag of extinction is required toward source D. The fact that the extinction toward sources A–C are consistent with that from interstellar material along the line of sight to the Galactic center, with no additional extinction from M-0.02-0.07, implies that the H II regions must indeed be close to the front surface of the molecular cloud. Similarly, the additional extinction seen toward source D confirms its location within M-0.02-0.07.

Assuming the extinction curve of Rieke & Lebofsky (1985), we expect both $A_{9.0}/A_{12.8}$ and $A_{10.5}/A_{12.8}$ to be 2.7. The extinction corrected Ar^{++} and S^{+3} abundances are then as given in Table 3, columns (10)–(11). The low fractional abundances of Ar^{++} indicate stellar temperatures $\approx 34,500$ – $36,500$ K (Rubin 1985), or spectral types O8–O9 (Panagia 1973). This

conclusion is entirely consistent with the spectral types derived from the required ionizing luminosities (Goss et al. 1985), and the IR to radio flux density ratio of source A (Yusef-Zadeh, Telasco, & Decher 1989), assuming each source is ionized by a single O star, although the substantial sensitivity of $[\text{Ar III}]$ to extinction makes our result somewhat uncertain. Indeed, the S^{+3} upper limit for source A suggests a slightly cooler stellar temperature, $T \lesssim 32,500$ K.

5. MOLECULAR CLOUD MODEL

Since the observed CS transitions sample only the denser parts of a molecular cloud, and since lower excitation transitions of various molecules show a cloud of even greater extent than is seen in CS (e.g., Liszt et al. 1985; Armstrong & Barrett 1985; Sandqvist 1989; Zylka 1990), a substantial amount of lower density gas must surround the structures seen in CS. With this inclusion the two dense CS features (the compressed shell around Sgr A East, and the peak to its east) can be interpreted respectively as (1) a compression wave moving into a more extensive cloud, and (2) an embedded dense core. (If this core is associated with the nearby compact H II regions, it may actually lie close to the front surface of the cloud—§ 4). The dense CS core, and the more extensive 40 – 50 km s^{-1} emission seen in CO (Liszt et al. 1985; Zylka et al. 1990; Zylka 1990), is then likely due to the undisturbed bulk of the cloud. Thus, in contrast to the model of Zylka et al., which superposes several clouds, it is possible to ascribe all of the $\approx 50 \text{ km s}^{-1}$ emission from the vicinity of M-0.02-0.07 to only one cloud, part of which has been disturbed by Sgr A East.

As discussed earlier, the 50 km s^{-1} molecular cloud exhibits a velocity gradient of about 5 – $6 \text{ km s}^{-1} \text{ arcmin}^{-1}$ in the declination direction. This gradient extends beyond the edge of the expanding Sgr A East shell (Fig. 4), making it clear that the gradient across the cloud is intrinsic to the cloud, and not related to the shell-cloud interaction. If interpreted as due to the cloud's rotation about the center, and extrapolated to a rotational speed of 110 – 180 km s^{-1} (Genzel & Townes 1987), the observed velocity gradient implies a galactocentric distance for M-0.02-0.07 of about 45 – 90 pc . Of course the cloud's orbit is likely not circular (Bally et al. 1988), implying that this distance estimate is very crude. Tidal stability arguments also place the cloud at greater than 30 pc from the center (Güsten & Henkel 1983). However, other distance estimates have tended to be smaller, for example, Mezger et al. (1989) and Genzel et al. (1990).

Since the observed CS shell is presumably compressed by the piston-like action of Sgr A East, this interaction should have left a kinematic signature on the molecular gas in the shell (e.g., Genzel et al. 1990; Ho et al. 1991). As Figure 9 shows (see

TABLE 3
IONIC RATIOS FOR THE SGR A EAST COMPACT H II REGIONS

Source (1)	15 GHz Flux (mJy) (2)	$\frac{\text{Ne}^+}{\text{H}^+}$ (3)	$\frac{\text{Ar}^{++}}{\text{H}^+}$ (4)	$\frac{\text{S}^{+3}}{\text{H}^+}$ (5)	$\frac{\text{Ne}^+}{\text{Ne}}$ (6)	$\frac{\text{Ar}^{++}}{\text{Ar}}$ (7)	$\frac{\text{S}^{+3}}{\text{S}}$ (8)	$A_{12.8}$ (mag) (9)	$\frac{\text{Ar}^{++}}{\text{Ar}}$ (corr) (10)	$\frac{\text{S}^{+3}}{\text{S}}$ (corr) (11)
A.....	570	6.2 (–5)	1.1 (–7)	<3 (–9)	0.39	0.012	<5 (–5)	1.0	0.14	<6 (–4)
B.....	173	5.8 (–5)	1.2 (–7)	...	0.36	0.013	...	1.1	0.20	...
C.....	245	4.7 (–5)	1.5 (–7)	...	0.30	0.016	...	1.3	0.41	...
D.....	95	0.9 (–5)	<1 (–8)	...	0.05	<0.001	...	3.3	<3.6	...

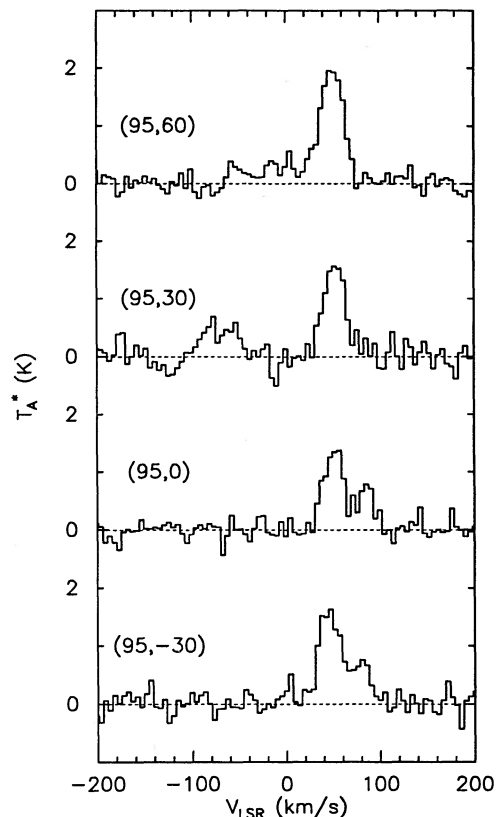


FIG. 9.—Four CS $J = 5-4$ spectra showing high-velocity emission. In addition to the main $40-50 \text{ km s}^{-1}$ emission component, the bottom two spectra show redshifted emission peaking at $80-85 \text{ km s}^{-1}$, and the top two spectra show blueshifted emission out to -100 km s^{-1} . The spatial offsets (in arcsec) are indicated in parentheses. The right ascension offset for all of the spectra is $95''$, placing this emission just inside (west) of the compressed CS shell (see Fig. 2).

also Fig. 1), the CS $5-4$ spectra confirm the presence of *both* highly blue- and redshifted emission components just inside of the Sgr A East shell. In the subset of spectra presented in Figure 9, all of which are located at $\Delta\alpha = 95''$, a highly blueshifted emission component is seen toward $\Delta\delta = 30''$ and $60''$, the emission at the former location extending to -100 km s^{-1} . This position is in good agreement with the location of the strongest blueshifted wing emission seen in C^{18}O spectra toward Sgr A East (Genzel et al. 1990). Furthermore, redshifted gas is seen in the two spectra immediately south of this location (Fig. 9), just where emission at redshifted velocities has been detected in NH_3 (Ho et al. 1991). However, the velocity of the redshifted component seen in these two CS spectra ($80-85 \text{ km s}^{-1}$) is significantly larger than is seen in NH_3 ($\approx 60 \text{ km s}^{-1}$). Finally, note that the blueshifts seen are significantly larger than the redshifts (from line center, the shifts are about -140 km s^{-1} vs. $+40 \text{ km s}^{-1}$).

The blueshifted emission region is also seen on Figure 2, as the small dashed contour near the center of the map. The redshifted region, which cannot be discerned on this map because of the vastly stronger 50 km s^{-1} emission, is just south of the location of this dashed contour. Both high-velocity emission components thus lie just inside of the compressed CS

ridge. (There are hints in the CS data that both emission regions extend somewhat further than the few spectra discussed indicate; however, the remainder of this emission is too weak, and too sparsely sampled, to draw any firm conclusions yet).

Since this high-velocity gas lies just inside of the compressed CS shell, it is possible to conclude that at least some of the molecular gas in the 50 km s^{-1} cloud has been accelerated to very high velocities by the impact of Sgr A East. Indeed, much of the dense CS ridge must have been accelerated to some extent, and thus its observed mundane velocity pattern (its aforementioned velocity gradient) implies that the compressed CS ridge lies, to a large extent, to the side of the expanding shell. This is consistent with its observed low covering factor (§ 2), and implies that the interaction region between the shell and the molecular cloud is narrow in projection. However, since both blue- and redshifted velocity components are present, some molecular gas must evidently be present on both the front and back sides of the expanding radio shell. Given the low shell covering factor, the observed asymmetric velocity shifts could then be due to asymmetric gas distributions on the front and back sides of the shell. Future more sensitive observations of this evidently narrow (in projection) interaction region should be able to reconstruct at least part of the velocity field, and so provide more reliable estimates of the energy in the Sgr A East shell (e.g., Mezger et al. 1989; Genzel et al. 1990).

6. SUMMARY

We have detected a dense swept-up CS shell in the M-0.02-0.07 molecular cloud. The projected shell follows the edge of Sgr A East for almost half its circumference, giving a convincing picture of the compression of the 50 km s^{-1} cloud by Sgr A East. Highly Doppler-shifted emission is found just inside of this shell, giving kinematic evidence for the acceleration of the molecular gas by the blast wave. The dense core of M-0.02-0.07, located just beyond the advancing compression wave, is as yet unaffected. Also beyond the reach of the compression wave are the compact H II regions A–D. They must thus predate the supernova explosion, and so Sgr A East cannot have been the “trigger” for their collapse into the star-formation phase. As was pointed out earlier, the short time scales involved also argue against Sgr A East as a triggering mechanism for star formation (e.g., Ekers et al. 1983, Mezger et al. 1989). Rather, the compact H II regions must be the result of an earlier episode of massive star formation. Observations of IR fine-structure lines indicate that the excitation of the ionized regions is consistent with the presence of a single O8–O9 star in each of the compact H II regions, and IR extinction arguments suggest that these star formation sites are located close to the front surface of the molecular cloud.

We wish to thank E. Sutton for acquiring a number of preliminary spectra, D. Chumney and the staffs of the CSO and IRTF for assistance with the observations, R. Güsten for acquiring the C^{34}S spectrum, and R. Zylka, M. Morris, P. G. Mezger, and R. Güsten for helpful comments. This work was supported by NSF grants AST90-15132 and AST90-20292, and the Texas Advanced Research Program.

REFERENCES

- Armstrong, J. T., & Barrett, A. H. 1985, *ApJS*, 57, 535
- Bally, J., Stark, A. A., Wilson, R. W., & Henkel, C. 1988, *ApJ*, 324, 223
- Becklin, E. E., Matthews, K., Neugebauer, G., & Willner, S. P. 1978, *ApJ*, 220, 831
- Blake, G. A., Sutton, E. C., Masson, C. R., & Phillips, T. G. 1987, *ApJ*, 315, 621
- Brown, R. L., & Liszt, H. S. 1984, *ARA&A*, 22, 223
- Ekers, R. D., van Gorkhom, J. H., Schwarz, U. J., & Goss, W. M. 1983, *A&A*, 122, 143
- Genzel, R., Stacey, G. J., Harris, A. I., Townes, C. H., Geis, N., Graf, U. U., Poglitsch, A., & Stutzki, J. 1990, *ApJ*, 356, 160
- Genzel, R., & Townes, C. H. 1987, *ARA&A*, 25, 377
- Goss, W. M., Anantharamaiah, K. R., van Gorkom, J. H., Ekers, R. D., Pedlar, A., Schwarz, U. J., & Zhao, J. 1989, in *IAU Symp. 136, The Center of the Galaxy*, ed. M. Morris (Dordrecht: Kluwer), 345
- Goss, W. M., Schwarz, U. J., van Gorkom, J. H., & Ekers, R. D. 1985, *MNRAS*, 215, 69P
- Güsten, R. 1989, in *IAU Symp. 136, The Center of the Galaxy*, ed. M. Morris (Dordrecht: Kluwer), 89
- Güsten, R., & Henkel, C. 1983, *A&A*, 125, 136
- Güsten, R., Walmsley, C. M., & Pauls, T. 1981, *A&A*, 103, 197
- Ho, P. T. P., Ho, L. C., Szczepanski, J. C., Jackson, J. M., Armstrong, J. T., & Barrett, A. H. 1991, *Nature*, 350, 309
- Ho, P. T. P., Jackson, J. M., Barrett, A. H., & Armstrong, J. T. 1985, *ApJ*, 288, 575
- Lacy, J. H., Achtermann, J. M., & Bruce, D. E. 1989a, in *IAU Symp. 136, The Center of the Galaxy*, ed. M. Morris (Dordrecht: Kluwer), 523
- Lacy, J. H., Achtermann, J. M., Bruce, D. E., Lester, D. F., Arens, J. F., Peck, M. C., & Gaalema, S. D. 1989b, *PASP*, 101, 1166
- Lester, D. F., Bregman, J. D., Witteborn, F. C., Rank, D. M., & Dinerstein, H. L. 1981, *ApJ*, 248, 524
- Liszt, H. S., Burton, W. B., & van der Hulst, J. M. 1985, *A&A*, 142, 237
- Lo, K. Y. 1989, in *IAU Symp. 136, The Center of the Galaxy*, ed. M. Morris (Dordrecht: Kluwer), 527
- Mezger, P. G., Zylka, R., Salter, C. J., Wink, J. E., Chini, R., Kreysa, E., & Tuffs, R. 1989, *A&A*, 209, 337
- Okumura, S. K., et al. 1989, *ApJ*, 347, 240
- Okumura, S. K., Ishiguro, M., Fomalont, E. B., Hasegawa, T., Kasuga, T., Morita, K.-I., Kawabe, R., & Kobayashi, H. 1991, *ApJ*, 378, 127
- Osterbrock, D. E. 1989, *Astrophysics of Gaseous Nebulae and Active Galactic Nuclei* (Mill Valley, CA: University Science Books)
- Panagia, N. 1973, *AJ*, 78, 929
- Pedlar, A., Anantharamaiah, K. R., Ekers, R. D., Goss, W. M., van Gorkom, J. H., Schwarz, U. J., & Zhao, J. 1989, *ApJ*, 342, 769
- Rieke, G. H., & Lebofsky, M. J. 1985, *ApJ*, 288, 618
- Rubin, R. H. 1985, *ApJS*, 57, 349
- Sandqvist, A. 1989, *A&A*, 223, 293
- Serabyn, E. 1984, Ph.D. thesis, Univ. California, Berkeley
- Serabyn, E., & Güsten, R. 1987, *A&A*, 184, 133
- Stark, A. A., Bally, J., Wilson, R. W., & Pound, M. W. 1989, in *IAU Symp. 136, The Center of the Galaxy*, ed. M. Morris (Dordrecht: Kluwer), 129
- Tsuboi, M., Handa, T., Inoue, M., Inatani, J., & Ukita, N. 1989, in *IAU Symp. 136, The Center of the Galaxy*, ed. M. Morris (Dordrecht: Kluwer), 135
- . 1991, preprint
- Yusef-Zadeh, F., & Morris, M. 1987, *ApJ*, 320, 545
- Yusef-Zadeh, F., Telesco, C. M., & Decher, R. 1989, in *IAU Symp. 136, The Center of the Galaxy*, ed. M. Morris (Dordrecht: Kluwer), 287
- Zylka, R. 1990, Ph.D. thesis, Univ. Bonn
- Zylka, R., Mezger, P. G., & Wink, J. E. 1990, *A&A*, 234, 133